Solution ^{1}H NMR Investigation of the Heme Cavity and Substrate Binding Site in Cyanide-Inhibited Horseradish Peroxidase†

Jeffrey S. de Ropp,‡ Pravat K. Mandal,§ and Gerd N. La Mar*,§

NMR Facility and Department of Chemistry, University of California, Davis, California 95616

Received September 2, 1998; Revised Manuscript Received November 16, 1998

ABSTRACT: Solution two-dimensional ^{1}H NMR studies have been carried out on cyanide-inhibited horseradish peroxidase isozyme C (HRP^C−CN) to explore the scope and limitations of identifying residues in the heme pocket and substrate binding site, including those of the "second sphere" of the heme, i.e. residues which do not necessarily have dipolar contact with the heme. The experimental methods use a range of experimental conditions to obtain data on residue protons with a wide range of paramagnetic relaxivity. The signal assignment strategy is guided by the recently reported crystal structure of recombinant HRP^C and the use of calculated magnetic axes. The goal of the assignment strategy is to identify signals from all residues in the heme, as well as proximal and distal, environment and the benzhydroxamic acid (BHA) substrate binding pocket. The detection and sequence specific assignment of aromatic and aliphatic residues in the vicinity of the heme pocket confirm the validity of the NMR methodologies described herein. Nearly all residues in the heme periphery are now assigned, and the first assignments of several "second sphere" residues in the heme periphery are reported. The results show that nearly all catalytically relevant amino acids in the active site can be identified by the NMR strategy. The residue assignment strategy is then extended to the BHA:HRP^C−CN complex. Two Phe rings (Phe 68 and Phe 179) and an Ala (Ala 140) are shown to be in primary dipolar contact to BHA. The shift changes induced by substrate binding are shown to reflect primarily changes in the FeCN tilt from the heme normal. The present results demonstrate the practicality of detailed solution ^{1}H NMR investigation of the manner in which substrate binding is perturbed by either variable substrates or point mutations of HRP.

Horseradish peroxidase (HRP[1], ∼44 kDa, monomeric with a single heme) carries out the one electron oxidation of aromatic substrates at the expense of H_2O_2 (*1*−*5*). It is one of the most intensively studied enzymes (*1*−*7*) and has served as a model for our current understanding of Michaelis−Menten kinetics. The absence (until recently) of a crystal structure for HRP had propelled it to the forefront of development of solution spectroscopic methods for elucidating electronic and molecular structural properties relevant to function (*8*−*14*). These studies have used as templates for comparison crystallographically characterized heme peroxidases, first cytochrome *c* peroxidase (C*c*P) (*15, 16*) and later plant peanut peroxidase, PNP (*17*). HRP has also proven a challenging candidate for the construction of homology models based on sequence homology to crystallographically characterized peroxidases (*18*−*20*). The available crystal structures, spectroscopic characterizations, and mutagenesis studies have identified the common location of the oxidizing equivalents in compounds I (Fe^{IV}═O and heme or amino acid radical) and II (Fe^{IV}═O) and the role of strongly conserved proximal (axial His, nearby Asp) and distal (Arg, His, nearby Asp) residues that facilitate the reduction of peroxides (*21*−*27*).

Spectroscopic methods had made less progress in defining the nature of the relatively nonspecific (*5*) aromatic substrate binding site of HRP. Early NMR studies excluded the metal as the binding site and instead placed the substrate 8−10 Å from the iron (*28*−*32*). A more detailed picture of the site was provided by suicide inhibition studies (*2, 33*) and transferred nuclear Overhauser effect studies, which located the substrate binding site at the edge of the heme near the pyrrole I/IV junction (*34*−*36*). Also, the ring of an aromatic residue has been located by NOEs near pyrrole IV, and one aromatic ring has been shown to be in dipolar contact with the substrate (*11, 37, 38*). Last, site-directed mutagenesis of aromatic residues believed important for substrate binding have shown that substitution of three of these Phe by Ala results in significant drop in substrate affinity, in the order Phe179 > Phe 68 > Phe 142 (*39*). The recent report of the crystal structure of nonglycosylated, recombinant resting state HRP^C in the absence and presence of the aromatic substrate,

† This research was supported by a grant from the National Institutes of Health, GM 26226. The NMR spectrometer utilized was purchased, in part, with funds provided by the National Institutes of Health (Grant RR-04795) and National Science Foundation (Grant BBS-88-04739).

* Corresponding author: Phone: (916) 752-0958. Fax: (916) 752-8995. E-mail: lamar@indigo.ucdavis.edu.

‡ NMR Facility.

§ Department of Chemistry.

[1] Abbreviations used: HRP, horseradish peroxidase; HRP^C, isozyme C of horseradish peroxidase; HRP^C−CN, cyanide ligated HRP^C; C*c*P, cytochrome *c* peroxidase; LiP, lignin peroxidase; BHA, benzhydroxamic acid; PNP, peanut peroxidase; 2D, two dimensional; NOE, nuclear Overhauser effect; NOESY, two-dimensional nuclear Overhauser spectroscopy; TOCSY, two-dimensional total correlation spectroscopy; DSS, 2,2-dimethyl-2-silapentane-5-sulfonate; ppm, parts per million.

10.1021/bi982125a CCC: $18.00
Published on Web 12/30/1998

benzhydroxamic acid, BHA (*40, 41*), now provides many structural details that will serve to both test the validity of the early models based on spectroscopic probes and provide another plateau on which to build with spectroscopy. The role of individual residues in enzyme activation, substrate binding, and substrate oxidation are now being determined by mutagenic, functional, and structural studies (*21*−*23, 27, 39, 42*−*45*). Complete understanding of the role of individual residues whose substitution impacts function will necessitate a description of the effects of the mutation on the orientation of conserved residues in each case. From the point of view of NMR spectroscopy, the signals of the majority of the residues in the active site must be assigned and the dipolar contacts between the residues and the substrate mapped, before effective solution structural studies can be launched on point mutants.

A particularly structurally informative derivative of HRP^C is the low-spin cyanide-inhibited form, HRP^C−CN, whose hexacoordinate state and distal ligand hydrogen bond models the activated states of HRP^C. The excellent spectral dispersion imparted to active site residues by the dipolar shifts due to the large paramagnetic anisotropy of low-spin iron(III) has enabled the development of a robust interpretative basis of the hyperfine shifts, which reflect subtle structural changes at the iron induced by remote substrate binding (*13*). The BHA:HRP^C−CN complex also shows the spectroscopically highly advantageous, but rare, situation where the dynamics of substrate binding are such as to allow the observation of transferred-NOEs between protein and substrate (*34*−*37*).

Our present study focuses on elucidating the substrate binding site in HRP^C−CN using ^{1}H NMR to answer the following questions: How well have the "first sphere" residues in contact with the heme been defined by previous solution NMR studies (*11, 12, 34, 36, 37, 39, 42, 45*−*48*) based on homology models from C*c*P (and more recently, PNP)? Is it possible with the crystal coordinates to unambiguously assign more remote residues (i.e., "second" or "third" sphere), in particularly those in the vicinity of the substrate binding site? How do the assignments and observed dipolar shifts reflect the interpretive bases developed on the basis of homology models? Can the dipolar contacts between HRP^C residues and BHA predicted by the crystal structure (*41*) be detected by solution ^{1}H NMR? Can solution NMR provide any details of structural changes induced by substrate binding? The answers to these questions will hopefully provide the basis for productive future NMR structural studies on mutant HRP^C−CN complexes using the crystal structure of HRP as a reference base.

EXPERIMENTAL PROCEDURES

Sample Preparation. Horseradish peroxidase isozyme C (HRP^C) was purchased from Boehringer-Mannheim as a lyophilized salt free powder and used without further purification. The sample concentration was 3 mM in 99.8% ^2H_2O. Cyanide ligation was achieved by adding 3 equiv of KCN (Mallinckrodt) to the protein solution. BHA (Sigma) was dissolved in ^2H_2O and added to the protein solutions to make substrate:protein complexes of BHA:HRP^C−CN, with BHA varying from 0.2 to 10 equiv. Spectra were obtained at varying substrate concentrations and sample temperatures to achieve optimal resolution of the numerous aromatic resonances important to this work; 1.4 equiv of BHA at a temperature of 55 °C provided the best overall resolution of the crowded aromatic window.

NMR Data. ^{1}H two-dimensional (2D) NMR data were obtained at 500 MHz on a GE-NMR Omega spectrometer. NOESY spectra (*49*) were collected in hypercomplex mode with a repetition rate of 1 s^{-1} over a 10 kHz spectral window, or in a few cases with a repetition rate of 3 s^{-1} over a 30 kHz spectral window, with 2048 data points in t_2 and 512 blocks of 128 scans in t_1. NOESY data were collected with mixing times of 35−200 ms as noted in the text and figure captions; the most informative spectra were obtained with 65 ms. WEFT-NOESY spectra (*11*) were obtained with a 35 ms mixing time and repetition rate of 3 s^{-1} to edit the NOESY spectrum to emphasize paramagnetic cross-peaks. CLEAN-TOCSY spectra (*50*) were recorded with 12, 20, and 40 ms spin lock times at repetition rates of 5 or 1 s^{-1}. Data were processed on a SGI Indigo-2 using MSI Felix software (version 97.0). TOCSY and NOESY data sets were processed with 30−60° sine-bell-squared apodization in both dimensions. All data sets were zero-filled to 2048 × 2048 points and phase corrected in both dimensions.

Calculation of Dipolar Shifts. Using the coordinates of protons from the HRP crystal structure (*40*) a least-squares five-parameter fit of 15 previously assigned (*11*) protons of >1 ppm dipolar hyperfine shift was used to initially calculate the orientation of the magnetic axes and the values of the magnetic rhombic and axial anisotropies, in a manner described previously (*13, 51*). The resultant values were then used to calculate the predicted dipolar and total chemical shifts of all other protons in HRP using

$$\delta_{DSS}(\text{calc}) = \delta_{dia} + \delta_{RC} + \delta_{dip} \quad (1)$$

where δ_{DSS}(calc) is the total calculated shift, δ_{dia} is the diamagnetic reference shift of a given proton with inclusion of any secondary structural effect (*52*), δ_{RC} is the calculated ring current shift (*53*) using the crystal structure coordinates, and δ_{dip} is the calculated hyperfine dipolar shift from the values of the magnetic axes and anisotropies and the atomic coordinates (*51*). Upon completion of all assignments the values of the magnetic axes and anisotropies were then further refined; see below.

RESULTS

Assignment Protocols. A large paramagnetic protein, for which isotope labels are not as yet available, necessarily restricts studies to proton-only methods for signals which show a degree of $\delta_{dip} + \delta_{RC}$ that shifts them away from the vast bulk of proton signals. Most readily characterized are aromatic and methyl-containing aliphatic residues in the vicinity of the heme (first and second sphere residues) whose $\delta_{dip} + \delta_{RC}$ enables their resolution from the remaining ~3 × 10^3 protons in HRP^C−CN. The residues in the first and second sphere of contact with the heme experience different degrees of paramagnetic relaxation, and differing acquisition (mixing times, recycle times, acquisition times) and processing (mainly apodization) conditions are needed to obtain the relevant data as discussed below. While the paramagnetic effect hinders 2D experiments by broadening lines and diminishing coherences, it provides key benefits by shifting select protons away from crowded spectral regions and by

imparting a variation in shift with $1/T$, which aids in validating cross-peaks (*54*).

The assignment protocol consists of identifying scalar and dipolar correlations of sufficiently resolved cross-peaks, confirming their presence at two temperatures (40 and 55 °C), and identifying likely assignments both from dipolar contacts predicted via the crystal structure and from comparison of the observed chemical shifts with those predicted by the magnetic axes via eq 1. Previous work on HRP^C−CN has generally yielded assignments (*11, 42, 55*) for residues in dipolar contact with well-resolved heme protons; here we extend assignments to additional residues not in contact with well-resolved heme protons and to residues not in dipolar contact with the heme at all (second sphere and beyond residues). Figures 1−3 and 5 present NOESY data relevant to important assignments in HRP^C−CN, while corresponding TOCSY data are available as Supporting Information. Table 1 lists peak labels and resultant assignments described below, observed chemical shifts, and calculated chemical shifts from eq 1; Figure 4 presents a schematic of the heme environment, dipolar contacts, and indicated assignments to be described herein.

Initial Calculation of Dipolar Shifts. The previous assignments (*11*) of 15 protons with $\delta_{dip} > 1$ ppm in the heme cavity of HRP^C−CN were used in conjunction with the coordinates of recombinant HRP^C to calculate the magnetic axes in HRP^C−CN. The resultant values[2] were $\alpha = 135°$, $\beta = 9.5°$, and $\kappa = 10°$. These preliminary values were used to guide further assignments; a final refinement was done upon completion of assignments (vide infra).

Strongly Relaxed Heme Peripheral Contacts. Previous studies of HRP^C−CN have identified R38, F41, F152, and I244 in contact with the heme (*11, 34, 42*). Most of these studies used large bandwidths and short acquisition, mixing, and recycle times to detect dipolar correlations between residues and heme protons outside the diamagnetic window, specifically the well-resolved heme 8-CH_3, 3-CH_3, and β-vinyl protons, at the expense of resolution in the region 10−0 ppm. In contrast, Figure 1 presents results of a WEFT-NOESY over a "small" bandwidth, 10 kHz, and with moderate mixing, acquisition, and recycle times. The WEFT technique edits to select strongly relaxed peaks, i.e., those of the heme and residues at its periphery (*11*). Previous assignments (*11, 34, 42*) are labeled in Figure 1 by heme position or residue label. Unassigned residues are labeled by capital letters,[3] and their proton signals by lower case letters with numbers, as shown in Table 1 and the figures.

Previously unreported correlations detected in Figure 1A are from the heme 5-CH_3 (in contact with β-meso) to the ring of F172, previously indirectly located via NOEs from the proximal α-helical NH connectivities (*11*). In addition, 5-CH_3 shows NOEs (in panels B and C) to two additional signals, one of which (labeled l3, Figure 1B) also has NOEs to F172. The signal labeled r2 at −0.17 ppm has a single TOCSY cross-peak at 2.41 ppm (Supporting Information); the AX spin topology is appropriate for an Ala. Inspection of the crystal structure indicates Ala 34 is the likely origin of the this AX system; this is further confirmed by the good agreement between the observed (strongly upfield shifted) and calculated chemical shifts, Table 1. (An expected NOE

Table 1: ^{1}H NMR Data for Selected Residues of HRP^C−CN

residue[a]	peak label	peak assignment	δ_{DSS} (obs)[b]	δ_{DSS} (cal)[c]	$\Delta\delta$ (BHA)[d]	Curie slope[e]
Ala 34 (R)	r1	αH	2.41	2.06	0	−0.64
	r2	CH_3	−0.17	−0.47	−0.07	−0.71
Leu 37 (L)	l1	NH	6.89	7.13	0.08	−0.42
	l2	αH	3.58	3.41	*f*	*g*
	l3	δ_2CH_3	1.33	0.65	*f*	−0.21
Leu 39 (O)	o1	NH	7.07	7.28	0.25	−0.21
Phe 45 (X)	x1	δ	7.00	7.37	0.02	0
	x2	ϵ	6.41	6.91	0.05	−0.21
	x3	ξ	4.91	4.97	0.14	−0.78
Phe 68 (A)	a1	αH	4.83	4.89	0.12	−0.07
	a2	ring H	7.76	7.62[h]	0.07	−0.21
Gly 69 (K)	k1	α_1H	5.30	5.43	*f*	1.06
	k2	α_2H	4.97	5.21	−0.10	0.99
Asn 70 (J)	j1	αH	6.27	5.84	−0.20	0.78
	j2	β_1H	3.32	3.47	−0.12	0.28
	j3	β_2H	3.16	3.46	−0.06	0.71
Ala 140 (M)	m1	αH	4.10	3.72	−0.43	*g*
	m2	CH_3	0.41	0.29	−0.30	−0.21
Phe 142 (B)	b3	δ	7.35	7.27	0	−0.14
	b1	ϵ	7.61	7.51	0.02	0.07
	b2	ξ	7.47	7.48	0.08	0
Phe 143 (F)	f3	δ	6.56	6.77	0	−0.28
	f2	ϵ	7.35	7.21	0	−0.07
	f1	ξ	7.43	7.30	0.03	0
Leu 148 (P)	p1	γH	1.27	1.04	0.03	*g*
	p2	δ_1CH_3	0.08	−0.14	0.04	−0.21
	p3	δ_2CH_3	−0.13	−0.58	0.01	−0.92
Phe 152		δ	7.17	7.06	0	−0.28
		ϵ	6.35	6.61	0	−0.64
		ξ	5.57	5.97	0	−1.06
Val 155 (S)	s1	γ_2H_3	−0.28	−0.45	0.08	−0.07
Leu 163 (T)	t1	γH	0.63	0.96	0	0.07
	t3	δ_1CH_3	−0.73	−0.93	−0.01	−0.57
	t2	δ_2CH_3	0.17	0.15	0	−0.21
Leu 166 (N)	n1	δ_2CH_3	0.55	0.40	0	−0.07
Phe 172		NH	9.44	9.29	−0.24	0.85
		αH	5.63	4.57	−0.09	0.14
		δ	7.64	7.44	−0.18	0
		ϵ	7.18	7.17	−0.10	−0.07
		ξ	6.59	7.02	−0.04	−0.28
Phe 179 (W)	w1	αH	4.88	4.36	0	−0.50
	w2	ring H	7.78	7.42[h]	0.02	0.07
Tyr 233? (Q)	q1	ϵ1	8.75	9.27	0.02	1.34
	q2	ϵ2	8.26	7.31	−0.07	1.06
	q3	δ1	6.56	8.80	−0.07	0.57
	q4	δ2	5.01	5.06	−0.09	0.35
Phe C	c1	ξ or δ	7.89		0	0.07
	c2	ϵ	7.45		−0.03	0.07
	c3	δ or ξ	7.04		−0.03	0.07
aromatic E	e1	δ	7.28	7.34[i]	0.02	0
	e2	ϵ	6.11	6.28[i]	0	−0.07

[a] Residue label with sequence assignment (where possible). [b] Observed chemical shift in ppm from DSS at 55 °C, pH 7.0. [c] Calculated chemical shift in ppm from DSS from eq 1 using δ_{dip} calculated from the magnetic axes. [d] Change in chemical shift with addition of saturating amount of BHA, extrapolated from change in shift with 1.4 equiv of BHA (0.8 of protein complexed). [e] Slope of Curie plot of observed chemical shift vs reciprocal absolute temperature, in units of ppm·K $\times 10^3$. [f] Spectral congestion and line broadening with addition of BHA precluded determination. [g] Chemical shift at lower temperatures could not be determined, hence, slope could not be calculated. [h] Average of δ and ϵ protons. [i] Calculated shift for Y234 protons (see text).

[2] The angles of the magnetic axes (*51*) are defined as follows: β is the tilt of the magnetic *z*-axis from the heme normal; α is the angle between the projection of the magnetic *z*-axis on the heme plane and a line drawn through the nitrogens of pyrroles I and III (see Figure 4A), with counterclockwise rotation taken as positive; κ is the angle between the projection of the rhombic magnetic axes on the heme plane and the nitrogen−nitrogen vector of pyrroles I and III.

[3] The labels of residues are chosen to match those of previous studies (*11, 37*).

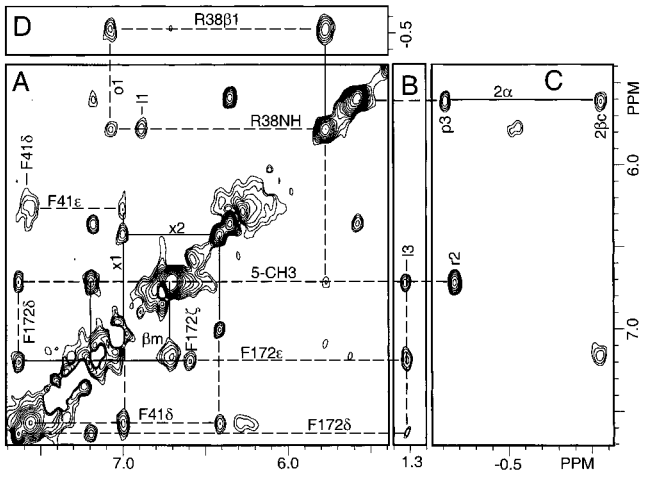

FIGURE 1: Portions of the 500 MHz WEFT-NOESY spectrum of HRP^{C}−CN in $^{2}H_2O$ at 55 °C, pH 7.0. Data were collected with a 35 ms mixing time and recycle time of 330 ms, with a postinversion delay of 150 ms. Solid lines show intraresidue dipolar contacts, and dashed lines connect interresidue cross-peaks. Intraresidue aromatic cross-peaks were confirmed by the corresponding TOCSY cross-peaks (Supporting Information). Peak positions are labeled with a lower case letter and number to indicate a proton of a specific residue (e.g. r2), except where previously assigned in which case the assignment is given explicitly (e.g. R38 NH). The cross-peak labeled βm is produced by the heme 5-CH:β-meso contact.

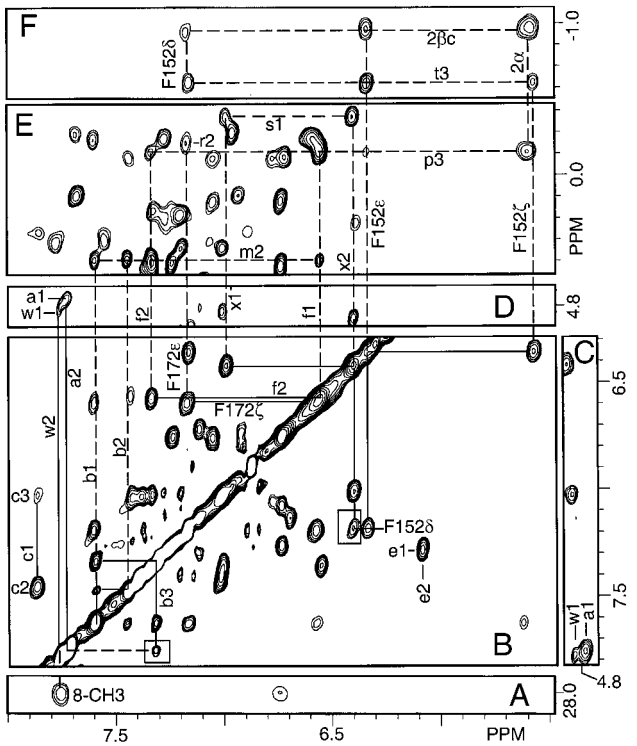

FIGURE 2: Portions of the NOESY spectrum (65 ms mixing time, 1 s recycle time) of HRP^{C}−CN in $^{2}H_2O$ at pH 7.0, 55 °C. Solid lines connect intraresidue cross-peaks, and dashed lines show interresidue contacts. Intraresidue cross-peaks were confirmed by corresponding cross-peaks in CLEAN-TOCSY spectra (Supporting Information). Aromatic ring systems are labeled (i.e., a−c, e, f, w, x) as described in the text except where previously assigned, where the residue number is given (i.e., F152, F172). Panel A presents a portion of the NOESY spectrum obtained with a 35 ms mixing time and 330 ms recycle time showing dipolar contact from the 8-CH_3 to the ring of Phe W (and not Phe A). (B) shows the aromatic region, (C) and (D) show contacts from aromatic to selected α protons, and (E) and (F) show aromatic−aliphatic contacts. In panel B the boxed x2:F152δ NOE was obtained at a lower contour; the boxed a2:b3 (Phe A:Phe B) NOE is obtained in a NOESY dataset with a 200 ms mixing time. (C) is presented to show that the cross-peaks from a2, w2 to a1, w1, respectively, can be clearly resolved in the F2 dimension.

to the 6βs is also observed, Figure 3A.) The signal l3 in Figure 1B is in too densely crowded a region to resolve its TOCSY cross-peaks unambiguously. However, the NOEs to 5-CH_3, F172, as well as to the heme 4αH (not shown) are unique in the crystal structure to L37 $C_{\delta 2}H_3$. 5-CH_3 also shows a weak NOE to the previously assigned R38 NH (*11*), Figure 1A. From R38 NH two additional NOEs (Figure 1A) are detected, one with a NOE to R38 $C_{\beta 1}H$, Figure 1D. Residues 32−44 of HRP exist in an α-helix (*40*), and this and the absence of any expected aromatic contacts from R38 NH indicate that the NOEs constitute the peptide connectivities of L37 NH−R38 NH−L39 NH; the latter is distinguished by the expected NOE from R38 $C_{\beta 1}H$. The assignments are summarized in Table 1 and Figure 4A,B.

The presence of these NHs after (in this case) many months in $^{2}H_2O$ solution is in keeping with the extraordinarily low lability of proximal and distal helix NHs previously noted (*11, 56*). Other interresidue NOEs of note in Figure 1A are from F41, previously assigned by an NOE from the 3-CH_3 (*11, 42*), to an aromatic spin system previously labeled X, which shows the three-spin TOCSY topology of a freely rotating Phe ring (Supporting Information). The only Phe in proximity to F41 is F45 and X is so assigned;[4] the strongly pronounced upfield shifts are well predicted, Table 1. One additional NOE of note is from 2α to a peak labeled p3 in Figure 1C, which will be treated further below.

Moderately/Weakly Relaxed Residues. For characterization of less strongly relaxed residues, a recycle time of 1 s and NOESY mixing times of 65 ms or greater were used. Figure 2 presents portions of the aromatic and aromatic to aliphatic regions of the NOESY spectrum of HRP^{C}−CN. Figure 2B shows the intraresidue contacts for six well-resolved aromatic three-spin (Phe) systems, B, C, F, X, F152, and F172, along with the two-spin aromatic system E. All intraresidue NOEs were confirmed by TOCSY correlations (Supporting Information). Spin systems B and E were first observed and labeled by Veitch (*37*), and system F was observed by Banci (*38*). No NOEs are noted between aromatic rings under these conditions except for X(F45):F152 in Figure 2B; this NOE is consistent with the crystal structure.

NOESY contacts from the aromatic region to the aliphatic (Figure 2F) are noted for F152 to 2β and to a peak t3, as previously observed (*11, 42*). The TOCSY spin topology for T is that of an upfield-shifted Leu/Val isopropyl group (Supporting Information). Similarly the residue P in contact with 2α (Figures 1C, 2E) shows a $(CH_3)_2CH$ TOCSY spin topology (Supporting Information). Leu/Val spin systems in proximity to pyrrole A are limited to L148 and L163. L148 and L163 show a common NOE in the upfield window, Figure 3A. L148 and L163 can be distinguished in that L148 $C_{\delta 2}H_3$ (p3) has a strong NOE to 2α but weaker to 2β with none to F152 (Figure 3A,B), while L163 $C_{\delta 2}H_3$ (t3) has NOEs to 2β and F152 but none to 2α (Figure 3A,B). The assignments fit the crystallographic data and the upfield shifts

[4] Phe X, with three upfield dipolar shifted rings protons, contrary to initial interpretation (*12*), does not exhibit NOESY cross-peaks to either 8-CH_3 or 7H_α.

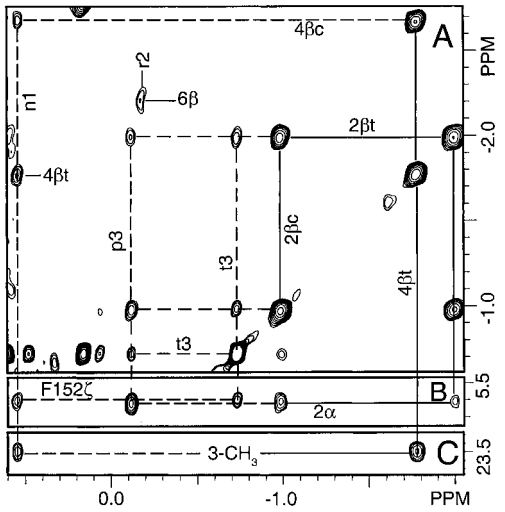

FIGURE 3: Portions of the aliphatic region of the NOESY spectrum (65 ms mixing time, 1 s recycle time) of HRP^C-CN in ^2H_2O at pH 7.0, 55 °C. Peak labels follow the convention of Figures 1 and 2. Solid lines label intraresidue cross-peaks, and dashed lines show indicate interresidue contacts. Intraresidue cross-peaks were confirmed by corresponding cross-peaks in CLEAN-TOCSY spectra (not shown; Supporting Information). (C) shows a section of the 35 ms mixing time, 330 ms recycle time NOESY spectrum of HRP^C-CN.

of both L148 and L163 fit well with the predicted shifts utilizing the magnetic axes, Table 1.

From p3, the L148 $C_{\delta 2}H_3$, two additional moderate NOEs (Figure 2E) are noted to peaks f1 and f2 of Phe F; the only realistic candidate from the crystal structure is F143. In addition, peaks f1, f2, and f3 all show NOEs to a peak m2, which also has NOEs to peaks b1 and b2, Figure 2E. The TOCSY spin topology of M cannot be definitively resolved under these conditions, but in the presence of BHA it shifts upfield (vide infra) far enough that an AX type TOCSY spin system consistent with an Ala is clearly revealed. The only Ala in appropriate proximity to Phe 143 is A140 and system M is so assigned (Table 1); it then follows that Phe B is the nearby F142. An interresidue F142:F143 cross-peak is not observed here, perhaps due to the fact b2/f3 and b3/f2 are very close in chemical shift, but is observed in the presence of BHA (vide infra). The chemical shifts of both F142 and F143 are well predicted, Table 1.

Other aromatic:aliphatic contacts of note are F172 to r2, the A34 CH_3 (Figure 2E), and X(F45) to an upfield shifted peak labeled s1, Figure 2E. The peak s1 is part of the TOCSY spin pattern of a Val (Supporting Information) and is assigned to V155, which has the appropriate upfield predicted shift (Table 1) and contact to F45. One additional aliphatic peak can be assigned as shown in Figure 3. An upfield shifted signal at 0.55 ppm denoted n1 with NOEs to 3-CH_3, F152ζ, and both 4βs can only be L166 $C_{\delta 2}H_3$; an elucidation of its TOCSY spin system was not possible. Assignments are summarized in Table 1 and Figure 4A.

Previous work by Veitch (*37*) had detected a NOESY cross-peak from an aromatic system denoted A to Phe B, while 8-CH_3 was shown to be in contact with an aromatic system labeled W (*11*, *39*), as noted in Figure 2A,B. The chemical shifts of the ring protons of A and W, a2 and w2, respectively, are very similar (Figure 2B, Table 1) but can be distinguished by their NOEs to peaks a1 and w1 in Figure

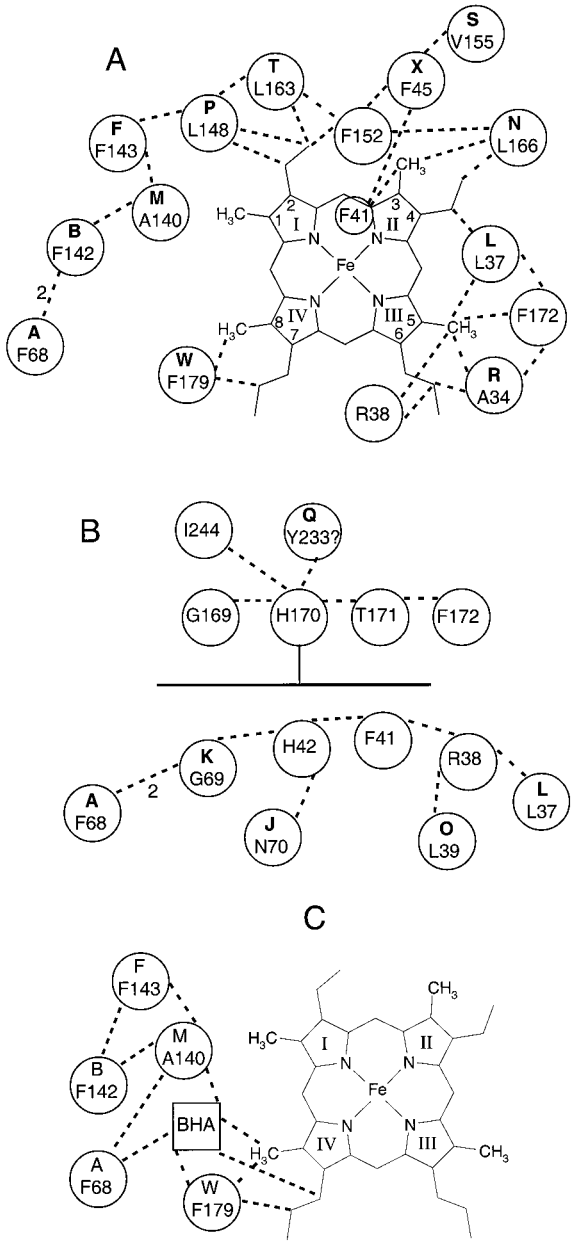

FIGURE 4: Summary of the NMR detected dipolar contacts in HRP^C-CN, presented as a schematic diagram of the heme and substrate binding pockets of HRP^C-CN, based on crystallographic data and NMR data. (A) shows the face-on view of heme and heme periphery of HRP^C-CN in the absence of BHA. (B) shows the edge-on view of heme and proximal (top) and distal (bottom) residues; view is approximately through the heme $\alpha-\gamma$ mesos. (C) BHA:HRP^C-CN complex, face-on view. (C) presents only those contacts near the BHA binding site; the magnitude of NOESY cross-peaks indicate the rest of the contacts in (A) and (B) are unchanged when BHA is complexed. Previously assigned residues (*11*, *34*, *39*, *42*, *56*) are labeled by their sequence position only, and presently identified residues are labeled both by the upper case letter code and sequence position following assignment. Dipolar contacts determined herein or previously are indicated by dashed lines. Heme pyrroles are labeled with Roman numerals. A "2" by a dashed line indicates a likely secondary NOE. For clarity in (A) the I244 in contact with 8-CH_3 (*11*, *42*) is omitted, but I244 is included in (B); the H42 to BHA NOE (*35*, *36*) is omitted to simplify (C).

2D (which are likely intraresidue NOEs to the respective α protons). The W and A rings do not show TOCSY cross-peaks (Supporting Information), but in the resting state form of the protein both A (in contact with Phe B) and W (in

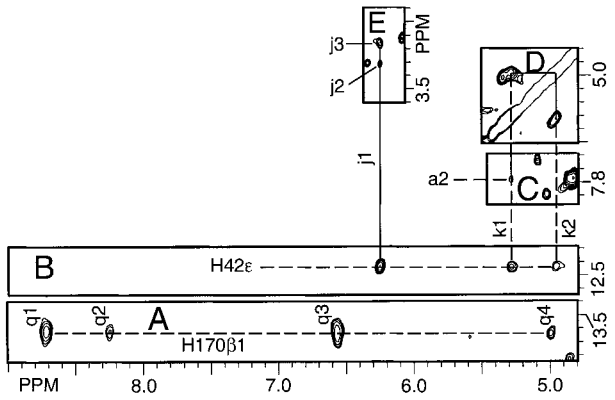

FIGURE 5: Portions of the NOESY spectrum (65 ms mixing time, 1 s recycle time) of HRP^{C}−CN in $^{2}H_2O$ at pH 7.0, 55 °C, showing relevant dipolar contacts in the proximal and distal environments of the heme. Peak labels follow the convention of previous figures. Panel C was obtained with a 200 ms mixing time and 1 s recycle, necessary to produce the (secondary) k1 to Phe A NOE.

contact with 8-CH_3) have been shown to be aromatic three spin systems (*14*, *37*), characteristic of Phe. Apparently in the cyano-ligated state all three spins of both rings are of similar shift and intraresidue NOESY/TOCSY cross-peaks cannot be detected.[5] In the present work an A/B NOE is detected, but only at long (200 ms) mixing time, indicating the NOE is likely secondary, Figure 2B. Residue W, in contact with 8-CH_3, has been assigned by Veitch to Phe 179 (*39*), while Phe A is not assigned. Two remaining well-resolved spin systems in Figure 2B are C (a three-spin Phe) and the two-spin system E, possibly a Tyr; neither shows NOEs to the heme or other assigned resonances.

Residues in Contact with Distal Histidine. The distal His in HRP^{C}−CN was assigned previously by analysis of dipolar shifts of the ring protons and 1D NOEs (*34*); it has no NOEs to the heme but does to F41 and to a peak previously labeled j1 at fast recycle times and short mixing times (*11*). With a 65 ms mixing time and 1 s recycle the distal H42 CϵH shows NOEs not only to j1 but also to two peaks we label k1 and k2, Figure 5B. Peaks k1 and k2 have NOESY (Figure 5D) and TOCSY (Supporting Information) cross-peaks between them; the spin topology and chemical shift is indicative of a Gly. The dipolar contacts and predicted shift assign the Gly as G69, Table 1. The j1 signal shows NOESY (Figure 5E) and TOCSY (Supporting Information) cross-peaks to two peaks j2 and j3 near 3.3 ppm, indicative of a $C_\alpha H-C_\beta H_2$ fragment. The very large downfield shift of the $C_\alpha H$ proton is predicted for N70 (Table 1), which has the appropriate proximity to H42. Additionally, at 200 ms mixing time the G69 $C_\alpha H$ proton shows a weak and likely secondary NOE to the Phe A ring signal (Figure 5C), which from the crystal structure could only occur if Phe A *is F68*. Accordingly Phe A is assigned as F68, Table 1.

Residues in the Proximal His Environment. Experiments at fast conditions have detected NOEs from the proximal H170 to the I244 (*34*) (which is also in spatial contact with 8-CH_3), from the H170 NH to the adjacent G169 and T171 NHs, and from the H170 β_1H to a four-spin system denoted Q (*11*); these NOEs are summarized in Figure 4B. Along with the F172 (also in contact with 5-CH_3; vide supra), this is a total of five assigned residues identified in the proximal environment, plus Q. Figure 5A shows under slow repetition conditions the NOEs from H170 β_1H to the four Q spins, all of which are TOCSY connected even at very short (12 ms) mixing time (Supporting Information). The crystal structure indicates two aromatic rings that could account for the Q system, Y233 and F221, located on either side of the proximal His ring. However, F221 is much closer to the iron. The TOCSY cross-peaks of Q are present even at 40 ms spin lock time (not shown) and are not indicative of a strongly relaxed spin system close to the iron; see Discussion. Thus the most likely assignment of Q at this time is the ring of Y233.

[5] At least two peaks for the Phe W ring are revealed following resolution enhancement of the one-dimensional NOE from the 8-CH_3 (*34*).

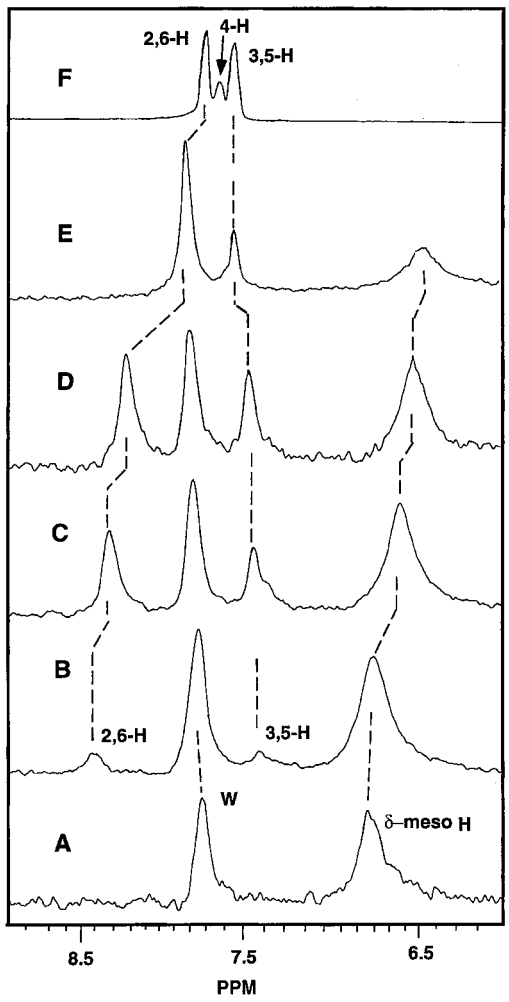

FIGURE 6: Observation of ring BHA resonances. (A−E) shown portions of the one-dimensional NOE difference spectra of BHA: HRP^{C}−CN, saturating (for 100 ms) the heme 8-CH_3 resonance at 28.02 ppm, for samples with BHA/HRP^{C}−CN molar ratios of (A) 0, (B) 0.2, (C) 0.4, (D) 1.4, and (E) 10. (F) shows the reference spectrum of BHA. The dashed lines connect the position of the averaged BHA resonances. Note that the NOEs are negative; the peaks have been phased upright to match panel F.

BHA Binding Site. The crystal structure of BHA complexed with recombinant HRP^{C} has recently been reported (*41*). Here are reported spectroscopic results on the HRP^{C}−CN:BHA complex in solution. Figure 6 shows a titration of HRP^{C}−CN with BHA, visualized as difference spectra obtained by 1D NOE irradiation of the heme 8-CH_3, known to be in dipolar contact with BHA (*56*). The difference spectra offer the advantage of uniquely identifying the

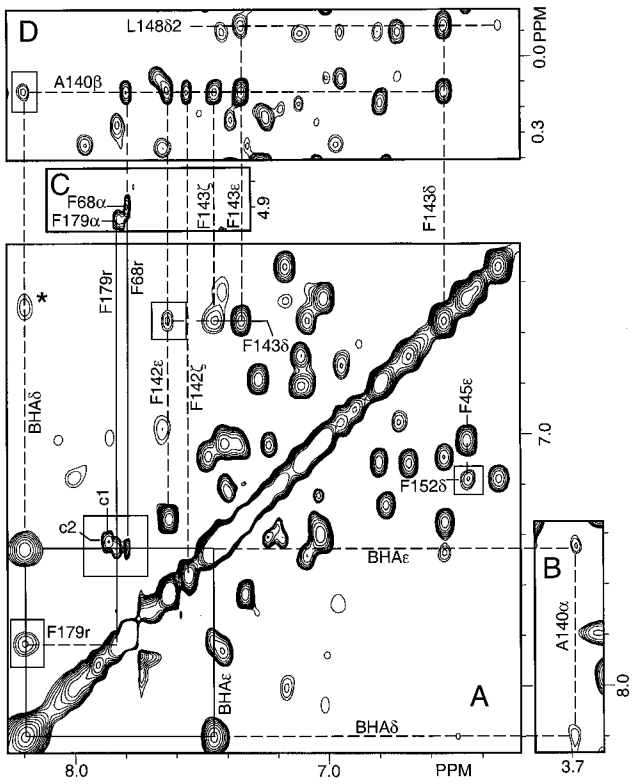

FIGURE 7: Portions of the NOESY spectrum (65 ms mixing time, 1 s recycle time) of BHA:HRP^{C}−CN at pH 7.0, 55 °C with 1.4 molar equiv of BHA. Peaks are now labeled for clarity with assignments determined and listed in Table 1. To simplify the figure, aromatic ring intraresidue cross-peaks are generally not labeled (these are easily detected in a corresponding TOCSY spectrum, Supporting Information). BHAϵ and BHAδ denote the BHA ring 3,5-H and BHA ring 2,6-H protons, respectively. The ring protons of F68 and F179 are labeled F68r and F179r, respectively. Boxed inserts are the same data, but plotted at lower contours, except for the box showing the BHA 3,5-H to F179r, F68r NOEs. The latter was processed with different apodization to resolve the cross-peaks. The peak marked with an asterisk is the q2/q4 cross-peak, degenerate here with BHA 2,6-H but resolvable at other temperatures.

substrate peak positions at any BHA concentration. Figure 6 clearly shows that BHA is in fast exchange between bound and unbound states. The large negative BHA peaks in the difference spectra are indicative of intermolecular transferred NOEs, reflecting the position of BHA in the substrate:HRP^{C}−CN complex. The BHA peaks in the difference spectra easily allow the assignment of the BHA shifts in 2D NOESY spectra; vide infra.

Figure 7 shows the NOESY spectrum of BHA:HRP^{C}−CN at 65 ms mixing time. Intraresidue cross-peaks of F142 (B), Phe C, E, F143 (F), F45 (X), F152, and F172 are detected by TOCSY results (Supporting Information) and define the chemical shifts of the various ring protons. Two interaromatic ring contacts are noted in Figure 7A. The F45:F152 NOE is detected, as in the substrate free protein, and with addition of BHA a F142:F143 NOE is now resolved. Figure 7D shows that F143 again produces NOEs to the L148$C_{\delta 2}H_3$ (in contact with 2α, not shown) and to A140 CH_3, which shifts upfield from 0.41 to 0.14 ppm with BHA addition. (The upfield shift of A140 CH_3 allows the resolution of its CH_α cross-peak in the TOCSY spectrum of BHA:HRP−CN; Supporting Information). The A140 CH_3 is also in dipolar contact to F142, Figure 7D, as is true for the uncomplexed HRP^{C}−CN.

New dipolar contacts, not seen in substrate free HRP^{C}−CN, are noted from *A140 CH_3 to F68 and BHA*, Figure 7D. The A140 CH_α proton also produces NOEs to BHA, Figure 7B. F68 and F179 have similar shifts, as in the substrate-free protein, but can again be distinguished from their NOEs to the respective CH_α protons, Figure 7C. Figure 7A shows that *BHA has NOEs to the rings of both F68 and F179*, in addition to the BHA NOEs to A140 noted above. No BHA NOEs to other aromatic rings are detected. A summary of the BHA:HRP^{C}−CN dipolar contacts is given in Figure 4C.

Comparing the data for comparable spectral windows in Figures 2 and 7 shows that BHA binding induces small shifts of several residues (summarized in Table 1) and an increase in the intensity of the NOEs between A140 CH_3 and F142, F143. *The latter indicates that the two aromatic rings are in closer proximity to A140 CH_3 in the BHA:HRP^{C}−CN complex*. The appearance of the F68 to A140 CH_3 NOE likewise indicates a limited structural change in the substrate bound relative to substrate-free complex.

Refined Magnetic Axes. Upon completion of assignments a refinement of the magnetic axes and anisotropies was done, using as input 23 single protons, 4 methyl groups, and one two-site ring chemical shift, all of which showed 1 ppm or greater of observed dipolar shift,

$$\delta_{\mathrm{dip(obs)}} = \delta_{\mathrm{DSS}}(\mathrm{obs}) - (\delta_{\mathrm{dia}} + \delta_{\mathrm{RC}}) \qquad (2)$$

with symbols defined as previously. The resultant five-parameter minimization yielded values of the magnetic axes of $\alpha = 138°$, $\beta = 10.5°$, and $\kappa = 2°$, with axial and rhombic magnetic anisotropies of 2.16×10^{-8} and -0.70×10^{-8} m^3/mol, respectively. Correlation between calculated and observed dipolar shifts is excellent (Supporting Information), with an error function of 0.065 ppm^2.

The magnetic axes were also calculated for the substrate bound BHA:HRP^{C}−CN complex. The results show the tilt of the major magnetic axis (β) decreases to 6.6°, indicating a corresponding decrease in the tilt of the cyanide ligand (*13, 51*).

DISCUSSION

Assignments in the Heme Periphery (Primary Sphere). The present study assigns protons of 15 residues of HRP^{C}−CN and provides new scalar or dipolar correlations for two others previously assigned. Beginning at the heme periphery, of the 18 residues within 3 Å of heme protons, 13 have now been at least partially assigned. This includes six in this work to add to earlier assignments using the C*c*P (primarily) and PNP homology models (*11, 39, 42, 56*). The assigned primary sphere residues are L37, R38, F41, A140, L148, F152, L163, L166, S167, G169, H170, F172, and F179.

Three of the five remaining primary sphere residues are adjacent to 1-CH_3 or the 6αHs, which are located in the densely crowded aliphatic region (*55*) and do not provide the resolution necessary for assignment even with WEFT methods. Overall the results indicate that studies tailored to detect a wide range of differential paramagnetic relaxivities can detect most of the residues in the primary sphere of HRP^{C}−CN. All of the residue assignments proposed earlier and reexamined here are confirmed except for the residue T, originally assigned (*12*) to L148 on the basis of compari-

son to the C*c*P crystal structure; the assignment of T is now corrected to L163 (Table 1). The remaining earlier assignments stand due to the structural similarity of C*c*P and HRP^C in some regions near the heme.

Assignments beyond the Heme Periphery. This study also locates nine residues in HRP^C−CN beyond the heme periphery (Figure 4A,B) and shows that assignments *can be extended beyond the first sphere contacts*. Key residues detected beyond the primary sphere include those of the substrate binding pocket, namely F68, F179, and A140, and the nearby F142 and F143. Additional second and third sphere resonances are also detected in the proximal and distal environments: L39, G69, and N70 (all distal) and Y233 (proximal).

Overall the NMR results identify almost all the key heme pocket residues, i.e., those of the proximal, distal, and substrate binding sites critical to catalysis, even without dipolar contacts to the heme scaffold for all residues. It is important to note that almost all of the residues which have been the subject of mutagenesis experiments (including R38, F41, H42, F68, N70, F142, F143, F172, F179) (*5, 21*−*23, 27, 39, 42, 43, 45, 46, 57*) are now assigned, and it can be expected that 2D ^1H NMR studies similar to these described herein should be able to address in some detail the effect of such substitution on adjacent residues.

Magnetic Axes. The initial limited assignments available from previous studies, with the HRP^C crystal coordinates, allowed formulation of "preliminary" magnetic axes which aided in further resonance assignment. The final refined magnetic axes enable excellent agreement between observed and predicted shifts (Table 1) and should be useful for NMR assignments in point mutants of HRP^C−CN. The refined magnetic axes show a tilt of the major magnetic axis of 10.5°, much less than the originally reported value of ∼20° (*13*). The original value was obtained by attempting to fit the magnetic axes to the coordinates of C*c*P, which led to the erroneously large tilt. The tilt value of 10.5° is still significant and would indicate a small tilt of the distal CN ligand away from the heme normal and toward the heme δ-meso. Both H42 and R38 have been proposed as residues to which the ligated cyanide hydrogen bonds (*56, 58*). The presently observed magnitude and direction of cyanide tilt is more consistent with hydrogen bonding to the distal His 42 N_ϵ in the crystal structure than to the Arg 38.

BHA Binding. The dipolar contacts observed in solution of F68, F179, and A140 to HRP^C−CN (Figure 7) are consistent with the crystal structure of the noncyanide ligated BHA:HRP^C complex (*41*) and are also consistent with a recent report of a molecular model of the BHA:HRP^C−CN complex (*59*). The increased intensity NOEs of F142, F143 to A140 in the BHA:HRP^C−CN complex relative to substrate-free HRP^C−CN are indicative of closer spatial proximity of the A140 CH_3 to these phenyl rings; such a marked change is not noted in the crystal structure of BHA:HRP^C relative to HRP^C. It cannot be ascertained at this time if the change in the A140 NOEs is an effect of ligation of CN to the iron in the present NMR study or an intrinsic difference between the crystal and solution environment of the substrate. It is noted that substrate binding is primarily relevant to HRP-I and HRP-II, although it is reasonable to presume that the substrate binding site is the same in the various derivatives. HRP and HRP-II differ both in the iron oxidation state and in the *protonation* state of the protein, with HRP-II modeled by HRP−CN, which, similar to HRP-II but in contrast to HRP, has a protonated His 42 (*56*). The differential affinity of HRP^C and HRP^C−CN for BHA has been attributed to the proton of the distal His 42 in the latter (*35*), and hence HRP−CN may model BHA binding to HRP-II better than does HRP.

The detection of the A140 CH_3 to F68 (Phe A) NOE in the presence, but not the absence, of BHA confirms the structural change noted in the crystal structure of BHA:HRP^C−CN, i.e., the movement of F68 on the B−C loop to bring this residue near to bound substrate (and A140). The BHA to F68, F179 (Phe A, Phe W) NOEs directly support the crystal structure results that these two aromatic rings are in proximity to BHA. While F143 is in the substrate binding "channel", no evidence of dipolar contacts from BHA to F143 are observed. Another NOE expected from the crystal structure would be G69 to BHA. The characteristic NOEs from H42ϵ to the G69α protons are greatly weakened with BHA addition, due either to line broadening or movement apart of the residues, and a BHA to G69 NOE could not be confidently ascertained.

The reduction in the magnitude of β, the tilt of the cyanide ligand, upon BHA binding agrees with earlier crude results using the C*c*P coordinates (*13*). Here the change is quantified as 4°, likely due to insertion of the polar edge of BHA into the distal heme environment toward the bound cyanide, as indicated by NOEs to the distal H42 (*35, 36*) as well as the crystal structure (*41*). The large change in chemical shifts of resonances not near the substrate, such as I244 $C_\delta H_3$ and R38 $C_{\beta 2}H$ (*34, 35, 47*), can be explained by the alteration of the magnetic axes noted here. Hence a change in chemical shift in itself is not definitive evidence of proximity of the substrate; dipolar contacts provide this.

Previously noted has been the wide variation in exchange rates of NH protons in the heme pocket, with the proximal H170 $N_\delta H$ and proximal and distal peptide NHs showing very slow exchange, while the distal H42 ring NHs show fast exchange (*11, 35, 56*). However, the postulated blocking of solvent access to the heme crevice upon BHA binding (*41*) correlates well with one other previously observed piece of NMR data, namely that exchange of the distal His ring NH protons is severely retarded in the BHA:HRP^C−CN complex (*35*).

Other Assignments. The assignments account for all aromatic residues in the vicinity of the heme except for F221, whose ring protons range from 4.6 to 7.2 Å from the iron in the crystal structure. F41 is approximately as close to the iron (on the opposite side of the heme) as F221, but under appropriate conditions of short mixing and recycle times F41 NOESY (*11*) (Figure 1A) and TOCSY cross-peaks (Supporting Information) can be discerned; we have not been able to observe such for F221. Equation 1 predicts the shifts of the F221 ring protons in the downfield region where the other aromatic rings are identified, yet no candidate exists. The ring protons of F221 are reasonably close to 8-CH_3, 7α, and I244 $C_\delta H_3$, all of which have been previously assigned (*42, 55, 60*), yet no NOESY cross-peaks from these protons to anything that could correspond to F221 have been identified. As stated before, the F221 ring is very close to the iron and hence its resonances would be broad, and if the ring is rotationally immobile due to proximity to the proximal H170

(as is implied by the crystal structure), this may render peaks so broad as to be undetectable.

Residue Q, likely Y233, shows unusual properties. First, it shows four spins, indicating that the Tyr ring is slowly rotating, unusual behavior for a ring in a protein. However, the homologous Phe 204 in LiP−CN, in dipolar contact with the proximal His βs, likewise shows a slowly rotating ring; all five spins are detected by TOCSY (*61*). The observed shifts of Q show moderate agreement with the predicted shifts of Y233, Table 1. The weak TOCSY cross-peaks between δ1H and δ2H, and between ϵ1H and ϵ2H (Supporting Information), are likely exchange cross-peaks (which are in phase with the TOCSY scalar correlation cross-peaks) from the slow rotation of the Tyr aromatic ring.

Tentative assignments of Phe C and the two-spin aromatic system E can be suggested. E shows large dispersion; hence, it is unlikely to have a hidden third spin, indicating it is a rapidly rotating Tyr ring. E has negligible Curies slopes (Table 1) indicating only slight paramagnetic shift; the large upfield shift of 6.11 ppm for one proton set must be due to a substantial ring current shift. Of the five Tyr in HRP−CN, only Y234 meets these criteria, and indeed the predicted shifts of Y234 show excellent correspondence to that of E, Table 1. E shows no NOEs to other assigned protons; hence, the assignment is only tentative.

Phe C shows appreciable chemical shift dispersion but only slight temperature dependence of the chemical shifts, Table 1. In addition the ϵ proton chemical shift position of Phe C (at 7.45 ppm) shows a weak NOE to the 4β protons (not shown), although it cannot be determined if the NOE is unique to Phe C. The only Phe expected to be in contact with 4β is F277. The predicted shifts of F277 (not shown) have qualitative agreement with those of Phe C, yet the lack of other NOEs to assigned protons leaves the assignment as only tentative.

Utility of Magnetic Axes and Predicted Shifts. The magnetic axes and chemical shifts calculated from eq 1 greatly aid assignments in a system as large as HRP^C−CN, with $\sim 3 \times 10^3$ protons. The calculated and observed shifts show excellent agreement in most cases (Table 1 and Supporting Information). The predicted shifts can winnow out incorrect assignments and, when ambiguity exists in dipolar contacts, aid in correctly identifying the residue producing the NOESY interaction.

The magnetic axes thus show general utility and successfully predict some unusual chemical shifts, such as the strong upfield shifts of the F45 and F152 rings and the L163 $C_{\delta 2}H_3$, and the strong downfield shift of N70 $C_\alpha H$, Table 1. The predicted shifts also account well for the lack of dispersion of the F68 ring protons. The calculated shifts are 7.63, 7.61, and 7.54 ppm for δ, ϵ, and ζ protons, respectively, and predict well the lack of dispersion and overall average downfield shift observed (Table 1 and Figure 2). F179 is also correctly predicted to have an averaged downfield shift with low dispersion. The magnetic axes should now greatly aid in the rapid assignment of the spectra of point mutants of HRP^C. Concomitantly, it should be possible to differentiate clearly whether mutation-induced shift changes for conserved residues result from reorientation of these residues or changes in the Fe−CN tilt that alter the magnetic axes orientation.

Routes to Other Assignments. Most residues in immediate proximity to the heme, and as yet unlocated, are adjacent to 1-CH_3 or 6α as mentioned above. Routes to identify these residues are available via reconstitution of HRP with selectively ^{13}C labeled 1-CH_3 (*62*) or 6α heme, in analogy to the use of deuterated hemes to make the early assignments in HRP^C−CN (*60*). With ^{13}C labels isotope editing methods can be employed to identify the protons in contact with these heme substituents.

The catalytically important Asp 247, with hydrogen bond to the proximal H170 ring, could not be located yet. NOEs from the H170 are not possible since the D247 (protonless) side chain is oriented to H170, placing respective protons too far apart. A route to assignment exists through the I244 side chain if those assignments (*11, 42*) can be extended to the I244 $C_\beta H$ proton, which is in proximity to the D247 C_β-Hs.

Conclusions. An effective strategy for assigning proton amino acid signals in the heme and substrate binding environments of HRP^C−CN has been developed. It encompasses the use of a wide range of mixing and recycle times in NOESY and TOCSY spectra and the use of calculated magnetic axes and predicted chemical shifts with the known crystal structure. Using this methodology, almost all residues in the heme periphery of HRP^C−CN have been assigned. Assignments have been extended beyond those residues in immediate contact with the heme and also include a number of residues in the proximal and distal environments. The NMR assignments include almost all catalytically relevant residues in the heme pocket, proximal and distal environments, and substrate binding site. The predicted chemical shifts from the magnetic axes determination greatly aid in making assignments. Several dipolar contacts of BHA to HRP^C−CN are identified in the BHA:HRP^C−CN complex. The dipolar contacts of the substrate binding site generally correspond well with the recent crystal structure of BHA:HRP^C, but a rearrangement involving A140 is detected by NMR that is not observed in the crystal structure. The binding of BHA produces a change in the magnetic axes of HRP^C−CN, reducing the tilt of the bound cyanide ligand. The ability to assign nearly all relevant residues will serve as an effective basis for study of point mutants of HRP^C−CN, where these methodologies will be able to provide detailed information on possible structural perturbations of the heme cavity and substrate binding sites.

ACKNOWLEDGMENT

We thank Professor A. T. Smith for kindly providing the crystal coordinates of HRP^C prior to their publication.

SUPPORTING INFORMATION AVAILABLE

Five figures (CLEAN-TOCSY spectrum of HRP^C-CN for aromatic residues; CLEAN-TOCSY spectrum of HRP^C-CN upfield Ala/Leu/Val groups; other portions of the CLEAN-TOCSY spectra for HRP^C-CN; portions of the CLEAN-TOCSY spectrum of BHA:HRP^C-CN; plot of calculated vs observed dipolar shifts with and without BHA) and one table (BHA shifts as a function of BHA/HRP^C-CN ratio) (6 pages). Ordering information is given on any current masthead page.

REFERENCES

1. Dunford, H. B. (1991) in *Peroxidases in Chemistry and Biology* (Everse, J., Everse, K. E., and Grisham, M. B., Eds.) pp 1−24., CRC Press, Boca Raton, FL.

2. Ortiz de Montellano, P. R. (1992) *Annu. Rev. Pharmacol. Toxicol 32*, 89−107.
3. English, A. M., and Tsaprailis, G. (1995) *Adv. Inorg. Chem. 43*, 79−125.
4. Poulos, T. L. (1993) *Curr. Opin. Biotechnol. 4*, 484−489.
5. Smith, A. T., and Veitch, N. C. (1998) *Curr. Opin. Chem. Biol. 2*, 269−278.
6. Welinder, K. G. (1992) in *Plant Peroxidases 1980−1990: Topics and Detailed Literature on Molecular, Biochemical, and Physiological Aspects* (Penel, C., Gaspar, T., and Greppin, H., Eds.) pp 1−24, University of Geneva, Geneva, Switzerland.
7. Welinder, K. G. (1992) *Curr. Opin. Struct. Biol. 2*, 388−393.
8. Andersson, L. A., and Dawson, J. H. (1990) *Struct. Bonding. 74*, 2−40.
9. Fidy, J., Paul, K.-G., and Vanderkooi, J. M. (1989) *Biochemistry 28*, 7531−7541.
10. Holzbaur, I. E., English, A. M., and Ismail, A. A. (1996) *J. Am. Chem. Soc. 118*, 3354−3359.
11. Chen, Z., de Ropp, J. S., Hernandez, G., and La Mar, G. N. (1994) *J. Am. Chem. Soc. 116*, 8772−8783.
12. de Ropp, J. S., Chen, Z., and La Mar, G. N. (1995) *Biochemistry 34*, 13477−13484.
13. La Mar, G. N., Chen, Z., Vyas, K., and McPherson, A. D. (1995) *J. Am. Chem. Soc. 117*, 411−419.
14. de Ropp, J. S., Mandal, P. K., Brauer, S. L., and La Mar, G. N. (1997) *J. Am. Chem. Soc. 119*, 4732−4739.
15. Poulos, T. L., and Kraut, J. (1980) *J. Biol. Chem. 255*, 8199−8205.
16. Finzel, B. C., Poulos, T. L., and Kraut, J. (1984) *J. Biol. Chem. 259*, 13027−13036.
17. Schuller, D. J., Ban, N., van Huystee, R. B., McPherson, A., and Poulos, T. L. (1996) *Structure 4*, 311−321.
18. Zhao, D., Gilfoyle, D. J., Smith, A. T., and Loew, G. H. (1996) *Proteins: Struct., Funct., Genet. 26*, 204−216.
19. Smith, A. T., Du, P., and Loew, G. H. (1995) in *Nuclear magnetic resonance of paramagnetic macromolecules* (Mar, G. N. L., Ed.) pp 75−93, Kluwer Academic Publishers, Dordrecht, The Netherlands.
20. Banci, L., Carloni, P., and Savellini, G. G. (1994) *Biochemistry 33*, 12356−12366.
21. Sanders, S. A., Bray, R. C., and Smith, A. T. (1994) *Eur. J. Biochem 224*, 1029−1037.
22. Newmyer, S. L., and Ortiz de Montellano, P. R. (1995) *J. Biol. Chem. 270*, 19430−19438.
23. Rodriguez-Lopez, J. N., Smith, A. T., and Thorneley, R. N. F. (1996) *J. Biol. Chem. 271*, 4023−4030.
24. Vitello, L. B., Erman, J. E., Miller, M. A., Wang, J., and Kraut, J. (1993) *Biochemistry 32*, 9807−9818.
25. Erman, J. E., Vitello, L. B., Miller, M. A., Shaw, A., Brown, K. A., and Kraut, J. (1993) *Biochemistry 32*, 9798−9806.
26. Choudhury, K., Sundaramoorthy, M., Hickman, A., Yonetani, T., Woehl, E., Dunn, M. F., and Poulos, T. L. (1994) *J. Biol. Chem. 269*, 20239−20249.
27. Smulevich, G., Paoli, M., Burke, J. F., Sanders, S. A., Thorneley, R. N. F., and Smith, A. T. (1994) *Biochemistry 33*, 7398−7407.
28. Burns, P. S., Williams, R. J. P., and Wright, P. E. (1975) *J. Chem. Soc., Chem. Commun.* 795−796.
29. Leigh, J. S., Maltempo, M. M., Ohlsson, P. I., and Paul, K. G. (1975) *FEBS Lett. 51*, 304−308.
30. Schejter, A., Lanir, A., and Epstein, N. (1976) *Arch. Biochem. Biophys. 174*, 36−44.
31. Morishima, I., and Ogawa, S. (1979) *J. Biol. Chem. 254*, 2814−2820.
32. Sakurada, J., Takahashi, S., and Hosoya, T. (1986) *J. Biol. Chem. 261*, 9657−9662.
33. Ator, M. A., and Ortiz de Montellano, P. R. (1987) *J. Biol. Chem. 262*, 1542−1551.
34. Thanabal, V., de Ropp, J. S., and La Mar, G. N. (1987) *J. Am. Chem. Soc. 109*, 7516−7525.
35. La Mar, G. N., Hernandez, G., and de Ropp, J. S. (1992) *Biochemistry 31*, 9158−9168.
36. Veitch, N. C., and Williams, R. J. P. (1991) in *Biochemical, molecular and physiological aspects of plant peroxidases* (Lobarzewski, J., Greppin, H., Penel, C., and Gaspar, T., Eds.) pp 99−109, University of Geneva, Geneva, Switzerland.
37. Veitch, N. C., and Williams, R. J. P. (1990) *Eur. J. Biochem. 189*, 351−362.
38. Banci, L., Bertini, I., Bini, T., Tien, M., and Turano, P. (1993) *Biochemistry 32*, 5825−5831.
39. Veitch, N. C., Gao, Y., Smith, A. T., and White, C. G. (1997) *Biochemistry 36*, 14751−14761.
40. Gajhede, M., Schuller, D. J., Henriksen, A., Smith, A. T., and Poulos, T. L. (1997) *Nat. Struct. Biol. 4*, 1032−1038.
41. Henriksen, A., Schuller, D. J., Meno, K., Welinder, K. G., Smith, A. T., and Gajhede, M. (1998) *Biochemistry 37*, 8054−8060.
42. Veitch, N. C., Williams, R. J. P., Bray, R. C., Burke, J. F., Sanders, S. A., Thorneley, R. N. F., and Smith, A. T. (1992) *Eur. J. Biochem 207*, 521−531.
43. Gilfoyle, D. J., Rodriguez-Lopez, J. N., and Smith, A. T. (1996) *Eur. J. Biochem. 236*, 714−722.
44. Howes, B. D., N., R.-L. J., Smith, A. T., and Smulevich, G. (1997) *Biochemistry 36*, 1532−1543.
45. Veitch, N. C., Williams, R. J. P., Bone, N. M., F., B. J., and Smith, A. T. (1995) *Eur. J. Biochem. 233*, 650−658.
46. Veitch, N. C. (1995) *Biochem. Soc. Trans. 23*, 232−240.
47. Veitch, N. C., and Williams, R. J. P. (1995) *Eur. J. Biochem. 229*, 629−640.
48. Veitch, N. C., Gao, Y., and Welinder, K. G. (1996) *Biochemistry 35*, 14370−14380.
49. Macura, S., and Ernst, R. R. (1980) *Mol. Phys. 41*, 95−117.
50. Griesinger, C., Otting, G., Wuthrich, K., and Ernst, R. R. (1988) *J. Am. Chem. Soc. 110*, 7870−7872.
51. Emerson, S. D., and La Mar, G. N. (1990) *Biochemistry 29*, 1556−1566.
52. Wishart, D. S., Sykes, B. D., and Richards, F. (1991) *J. Mol. Biol. 222*, 311−333.
53. Cross, K. J., and Wright, P. E. (1985) *J. Magn. Reson. 64*, 220−231.
54. La Mar, G. N., and de Ropp, J. S. (1993) *Biol. Magn. Reson. 12*, 1−78.
55. Thanabal, V., de Ropp, J. S., and La Mar, G. N. (1987) *J. Am. Chem. Soc. 109*, 265−272.
56. Thanabal, V., de Ropp, J. S., and La Mar, G. N. (1988) *J. Am. Chem. Soc 110*, 3027−3035.
57. Tanaka, M., Nagano, S., Ishimori, K., and Morishima, I. (1997) *Biochemistry 36*, 9791−9798.
58. Al-Mustafa, J., and Kincaid, J. R. (1994) *Biochemistry 33*, 2191−2197.
59. Chang, Y. T., Veitch, N. C., and Loew, G. H. (1998) *J. Am. Chem. Soc. 120*, 5168−5178.
60. de Ropp, J. S., Mar, G. N. L., Smith, K. M., and Langry, K. C. (1984) *J. Am. Chem. Soc. 106*, 4438−4444.
61. Banci, L., Bertini, I., Pierattelli, R., Tien, M., and Vila, A. J. (1995) *J. Am. Chem. Soc. 117*, 8659−8667.
62. Smith, K. M., Fujinari, E. M., Pandey, R. K., and Tabba, H. D. (1986) *J. Org. Chem 51*, 4667−4676.

BI982125A